Experimental investigation of evanescence-based infrared biodetection technique for micro-total-analysis systems

Arvind Chandrasekaran
Muthukumaran Packirisamy
Concordia University
Department of Mechanical Engineering
Optical-Bio Microsystems Laboratory
1515 Street Catherine Ouest
Montreal, Quebec H3G 2W1
Canada

Abstract. The advent of microoptoelectromechanical systems (MOEMS) and its integration with other technologies such as microfluidics, microthermal, immunoproteomics, etc. has led to the concept of an integrated micro-total-analysis systems (μTAS) or Lab-on-a-Chip for chemical and biological applications. Recently, research and development of μTAS have attained a significant growth rate over several biodetection sciences, *in situ* medical diagnoses, and point-of-care testing applications. However, it is essential to develop suitable biophysical label-free detection methods for the success, reliability, and ease of use of the μTAS. We proposed an infrared (IR)-based evanescence wave detection system on the silicon-on-insulator platform for biodetection with μTAS. The system operates on the principle of bio-optical interaction that occurs due to the evanescence of light from the waveguide device. The feasibility of biodetection has been experimentally investigated by the detection of horse radish peroxidase upon its reaction with hydrogen peroxide. [DOI: 10.1117/1.3210766]

Keywords: micro-total-analysis systems; infrared; absorption; evanescence; silicon-on-insulator; waveguides; horseradish peroxidase; hydrogen peroxide.

Paper 08377R received Oct. 20, 2008; revised manuscript received Feb. 3, 2009; accepted for publication Feb. 11, 2009; published online Oct. 30, 2009.

1 Introduction

Target recognition for any analyte such as a chemical, biological or gas sample, is the key aspect for the success of micro-total-analysis systems[1–5] (μTAS) and Lab-on-a-Chip (LOC) devices. Apparently, the limiting factor in scaling down the dimensions of a μTAS is primarily set by the analyte detector or the sensing system,[6] which adds to the importance of a suitable detection system being well integrated with its microfluidic counterpart. Thus, the key to the success of biodetection with μTAS lies in the sensing unit.

The mechanical resonant type is one of the earliest sensing units studied for Microsystems-based biodetections by virtue of the vibrational property changes in the structure on the interactions with enzyme and antibody molecules. Electrochemical methods of detection reported in the literature[7] include potentiometric, conductimetric (measuring the ion conductivity), and amperometry (based on the oxidation or reduction currents of analytes at a working electrode). Enzymatic field effect transistors (EnFETs) and ion sensitive field effect transistors (ISFETs) are also incorporated into the sensing systems,[8] and impedance sensing methods have also been explored for μTAS. In all the just mentioned methods of biodetection, the most common feature observed is that a number of sensitive physical parameters are involved that would result in the variation of the biodetection with physical parameters. In electrochemical methods, the electrical characteristics of solutions are believed to play an important role in physiologic functions that involve protein-protein and charged ligand interactions.[9] This leads to drawbacks such as dependence on geometry of the cells being studied, which can be overcome through the development of suitable optical detection methods.

Integration of optics into the realm of biology[10] has found several important applications for the detection and quantification of chemical and biological specimens. Recently, a great deal of attention has been focused toward the development of microoptoelectromechanical systems (MOEMS)-based biosensors.[11–13] These MOEMS devices have been integrated with other complimentary functional modules such as microfluidics, microthermal, micromechanical, etc., to form integrated (μTAS), which have principal advantages of efficient and rapid biosensing, owing to their characteristics such as miniaturization, portability, enhanced SNR, high sensitivity, selectivity, reliability, etc.[14]

Several optical detection methods have been employed for biodetection within integrated μTAS. Absorbance study[15–18] is one of the earliest used biodetection techniques for μTAS; however, the method is not applicable to all species, because not all biomolecules contain the chromophores that can exhibit optical absorption. Fluorescence spectroscopy[19–22] is another common and convenient method of detection compat-

Address all correspondence to: Arvind Chandrasekaran, Department of Mechanical Engineering, Optical-Bio Microsystems Laboratory, Concordia University, 1515 St. Catherine Ouest, Montreal, QC H3G 2W1, Canada. Tel: (514) 8482424 x7098; Fax: (514) 8483175; E-mail: achandra@alcor.concordia.ca

1083-3668/2009/14(5)/054050/11/$25.00 © 2009 SPIE

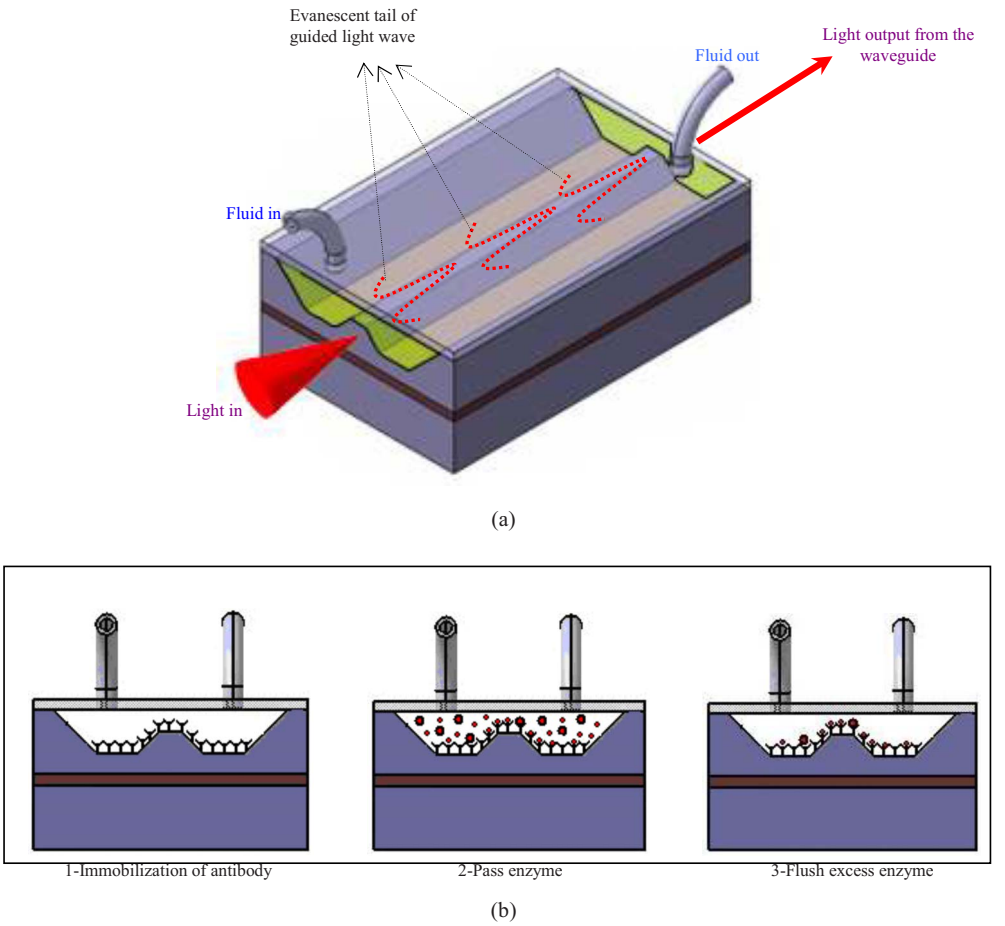

Fig. 1 Schematic illustration of evanescence wave detection using SOI waveguide in μTAS: (a) phenomenon of evanescence and (b) biodetection using evanescence.

ible with several μTAS applications and fluid actuation systems. To carry out fluorescence detection, however, it is important to tag the biomolecule with suitable fluorophore, which brings about the involvement of an additional processing step. Therefore, it is important to identify a suitable label free biodetection technique which can be employed for μTAS applications.

This paper proposes an infrared (IR) compatible detection technique on silicon and silicon-on-insulator (SOI) platforms for the sensing of chemical and biological specimen within μTAS.

This technique can also be integrated with the silica and polymer platforms. Herein, the biodetection was carried out through the bio-optical interaction brought about by the eva-

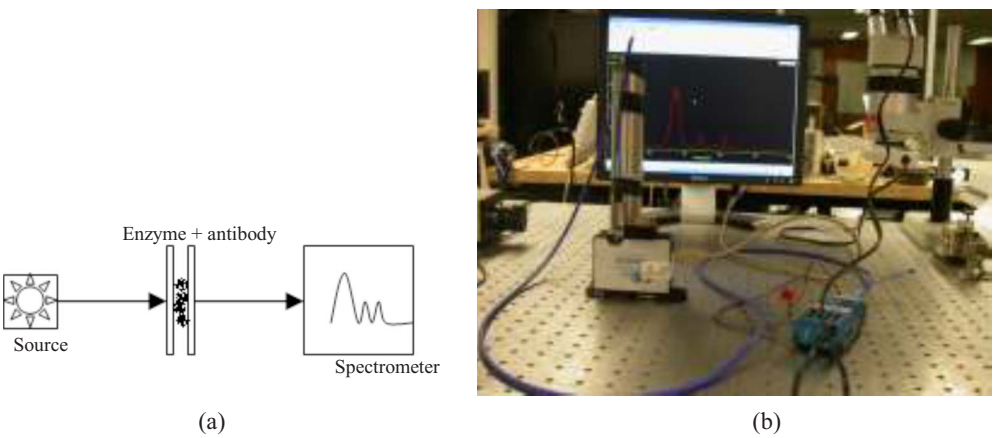

Fig. 2 (a) Schematic and (b) test setup of the optical absorption experiment at near UV wavelength.

nescence of light that is guided through a waveguide system. Figure 1 schematically illustrates the principle of μTAS. In a waveguide system, the optical field that is being guided through the waveguide depends on the optical properties of the cladding region and its geometry. Biological interactions that occur over the cladding region interact optically and influence the propagation of light through evanescent field. The induced loss due to this evanescence caused by the bio-optical interactions is studied in this paper.

Here, the evanescent tail that is emitted from the waveguide interacts with the biological specimen, which is immobilized on the surface of the waveguides, as shown in Fig. 1(b). This causes a perturbation of the guided wave, and by measuring this perturbation, one could decipher the nature of the bio-optical interaction and hence the characteristics of the biological specimen immobilized on the waveguide surface. The phenomenon of evanescence has been reported in literature[23] in the past, but surprisingly, this biodetection principle has not been much investigated on μTAS.[23]

To demonstrate the feasibility of biodetection using infrared photonics, in this work, horse radish peroxidase was chosen as the biomolecule and the enzyme was reacted with hydrogen peroxide, its antibody. Horse radish peroxidase (HRP) is a redox enzyme (biochemical catalyst) with an approximate molecular weight of 40 kDa (1 Da=1.660540×10^{-27} kg). It structurally resembles glycoprotein with one mole of protohaemin. These enzymes exhibit different isotropic forms and are generally isolated from the roots of horseradish.[24] When HRP comes into contact with selected substrate H_2O_2, it basically reduces the substrate. This reaction is spontaneous, within around[25] 200 μs. When the antibody is added to the enzyme, it produces superoxide or the ROS (reactive oxygen species) due to the reduction of hydrogen peroxide. In this process, H_2O_2 clings on to HRP and forms like a "cotton structure."[26] The main advantage of using HRP for testing is that its optical activity can be easily monitored and the activity is fairly stable in organic or inorganic solvents.[27]

The following sections of the paper give a detailed analysis of the characterization of the optical activity of the specimen, experimental investigation of the enzyme behavior through evanescence, and a summary of the results.

2 Characterization of the Optical Activity of Biomolecules

To understand the optical behavior of the HRP and H_2O_2, optical absorption measurements at different wavelengths were carried out. Essentially, the light was passed through a sample containing the enzyme and the antibody, and the optical behavior was monitored with respect to time. The time study of the bioreaction is important to analyze the developments and variations in the bioreaction characteristics. Here, three different optical spectrums at different wavelengths were used: blue light at 470 nm of the near-UV wavelength, red light at 635 nm for the visible wavelength, and IR light at 1550 nm.

The HRP used in these experiments is a commercial grade 9003-99-0 bought from Sigma, St. Louis, Missour, and the

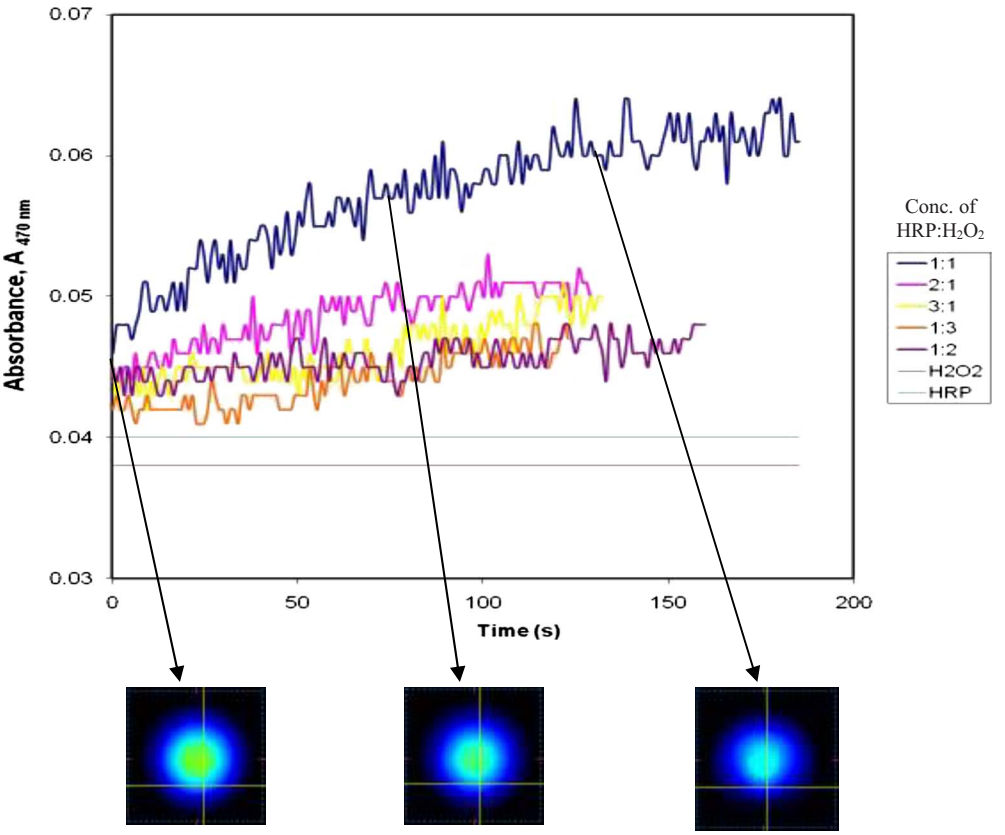

Fig. 3 Plot of time-varying absorbance at 470 nm for different volumetric ratios of HRP-H_2O_2.

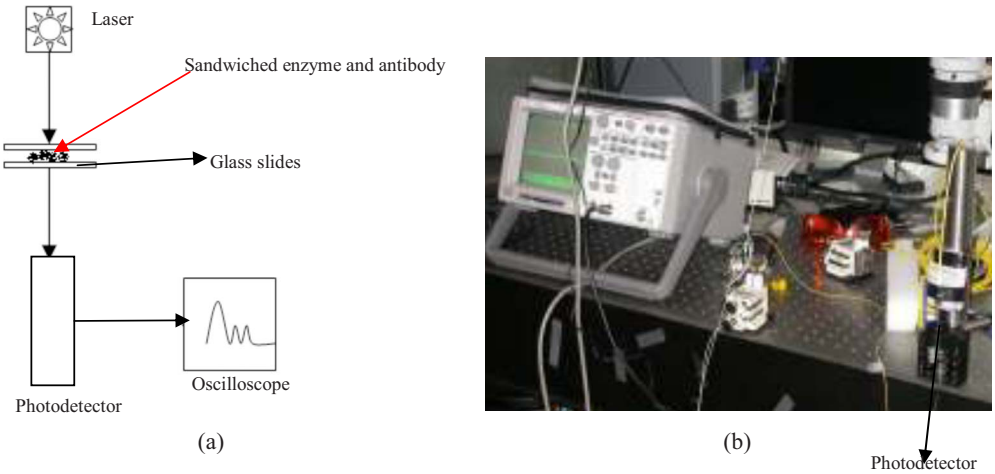

Fig. 4 (a) Schematic diagram and (b) test setup for absorption detection with light at 635 nm.

hydrogen peroxide is the standard grade bought from Sigma. The concentration of HRP used in all the experiments was 10 mg per 1 ml of 0.1-M phosphate buffer solution (PBS) at pH 6.0. The substrate H_2O_2 used was 30% by weight solution.

2.1 *Absorption Characteristics at* 470 nm

Figure 2 shows the experimental setup for this optical testing. It consisted of blue light emitted through a fiber optic bundle from a pulsed xenon lamp source at 470 nm. The light was coupled onto a spectrometer. The enzyme was taken in a micropipette and added to the substrate on a glass slide, and the slide was introduced in the slot available with the light source.

The absorbance measured by the spectrometer is given by the formula

$$A_\lambda = -\log_{10}\left(\frac{S_\lambda - D_\lambda}{R_\lambda - D_\lambda}\right), \tag{1}$$

where

λ = wavelength of light used
A_λ = absorbance
S_λ = intensity of light passing through the sample
D_λ = dark intensity
R_λ = intensity of light passing through a reference medium

Here, the glass slides were taken as the reference, and when the light was passed through plain glass samples, the reference intensity was noted. Dark intensity was measured when there is no light sensed by the spectrometer. However, to nullify the effects of the ambient conditions, the dark intensity was taken in the situation where the light source was switched off but the ambient light still was sensed by the spectrometer. Figure 3 is the plot of absorbance variation with time for different volumetric ratios of enzyme reactions. The variation in absorbance was also qualitatively studied and the corresponding images at different stages of optical absorbance due to the enzyme activities is indicated in the Fig. 3.

We can see that the absorbance is maximum when the enzyme is reacted with the antibody in the same volumetric concentration. When taken alone, the enzyme HRP exhibits a slightly higher absorption than the antibody for the same volume of 1 μl. As the volumetric concentration of any one of the specimens is increased during reaction, the absorption behaves similarly. Any further increase in concentration of either of the specimen moves the absorbance value closer to the value of HRP or H_2O_2 taken alone.

2.2 *Absorption Characteristics at* 635 nm

Figure 4(a) shows the schematic of the experimental setup with the red light of 635 nm wavelength. Figure 4(b) shows the test setup for this experiment. Since the spectrometer sensitivity was high for the visible light spectrum, a photodetector was used in this experiment. Pulsed light at 270 kHz was used and the output from the photodetector was studied using a standard oscilloscope (Agilent Technologies). A laser diode source (OZ Optics, Ontario) was used as the input of light through a fiber optic cable (Thor labs).

The procedure adopted for absorption measurement was as follows. The fiber from the laser source was initially aligned with respect to the photodetector. A glass slide was placed on top of the photodetector and was coated with antibody H_2O_2. Enzyme HRP was then added to the antibody and another glass slide was used to cover the assembly.

The output is obtained in terms of voltage given by the formula

$$V_0 = P_{\mathrm{pd}}\Re_\lambda R_L, \tag{2}$$

where

V_0 = measured output voltage
P_{pd} = power of input light in watts
$\Re_\lambda$ = resistivity of the photodetector measured in amperes per watt.
R_L = load resistance in the photodetector.

To convert the photocurrent into voltage, a load resistance of 50 Ω was added and the voltage reading was measured on the oscilloscope. The optical propagation loss with time for different enzyme ratios is as given in Fig. 5. We can see that equal volumetric ratio of HRP-H_2O_2 reaction produced the maximum absorption loss. However, H_2O_2 independently produced a slightly higher absorbance than the enzyme HRP

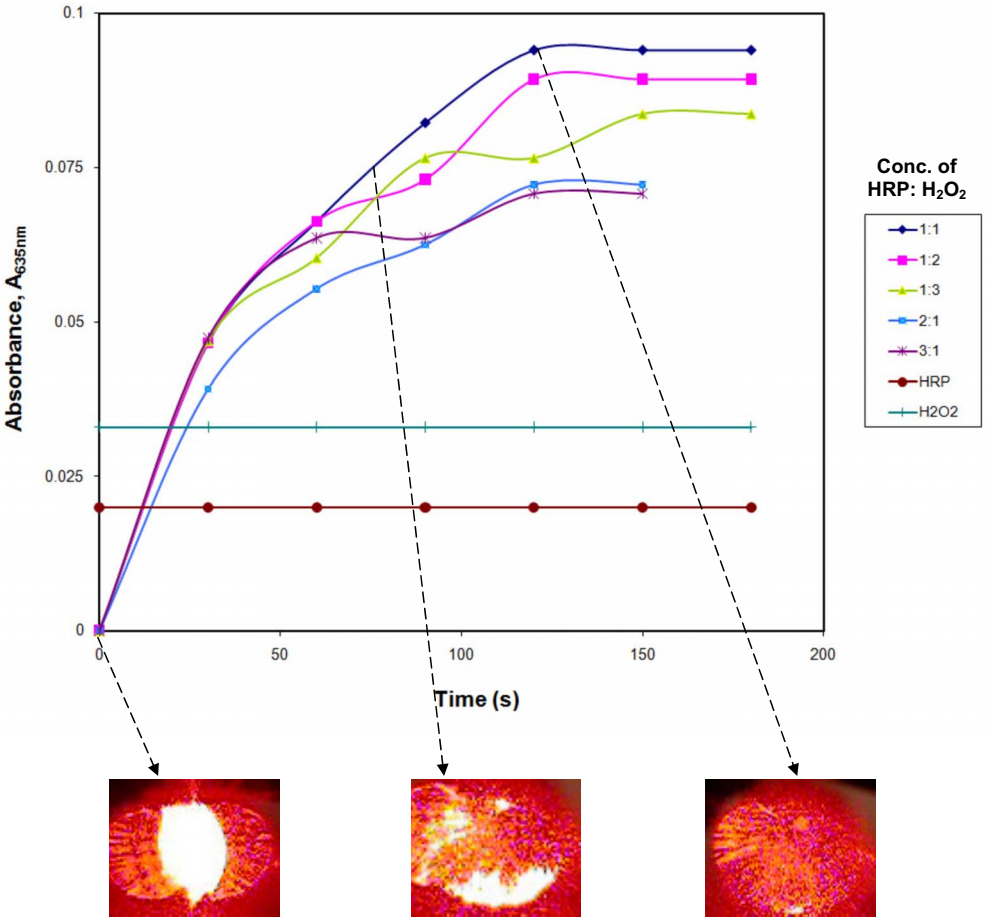

Fig. 5 Plot of absorbance variation with time measured with a photodetector for the reaction between HRP and H_2O_2 taken in different volumetric ratios at 635 nm wavelength.

at this wavelength range, and thus, the reaction between the two species produced more absorbance if the volumetric ratio of the antibody was higher.

2.3 *Absorbance Measurements at* 1550 nm *IR Wavelength*

A standard SMF28 fiber (Thorlabs, USA) was used as the input fiber for the IR light at 1550 nm (Photonetics Tunics BT external cavity laser) and a graded-index (GRIN)-lens-ended fiber was used as the collector fiber. An optical spectrum analyzer (OSA) (Agilent Technologies) was used to detect the light signals from the GRIN lens ended fiber. The input fiber and the output fiber were fixed vertically on a clamping arm that was mounted on two independent *xyz* micropositioners. This setup not only enabled placing the glass slide directly on top of the clamping arm holding the GRIN lens, but also the addition of the bio samples directly on top of the glass slide to measure instantaneous output readings. The experimental setup for the absorption measurement using infrared source is as shown in Fig. 6(b), the schematic for which is shown in Fig. 6(a).

The initial calibration of the OSA was carried out with reference to the laser source. The biological samples were added on the glass slide individually and the behavior of the samples was observed. Thereafter, the peroxide as added on top of the glass slide and after the addition of HRP, the slide was closed with another glass slide and the readings were recorded. Figure 7 gives the plot of optical loss with time for the individual species. Here, the absorbance is defined as $A_\lambda = -\log(P_t/P_0)$, where P_t is the power of light transmitted through the glass slides and P_0 is the power of input light. The reference value of optical power was taken as the amount of light passing through glass slides without enzymes. We can observe that the loss is maximum when the enzyme and the substrate are added in the same volumetric concentration. Here, with the IR light, the HRP exhibits more absorption than H_2O_2. At around 40 s, the absorption can be seen to be increasing, and then after some time, the absorption decreases again. This sudden increase in absorption could be because of the formation of intermediate compounds during the reaction, as reported by Baek and Van Wart.[28] After ~150 s of the reaction, the absorption trend irrespective of the concentration tends to be similar, which suggests the end of the reaction. This reaction time between the specimens is the same as predicted by the authors with a microfluidic microreactor setup.[29]

2.4 *Calculation of Absorption Coefficients*

The absorption coefficient was computed for the optical loss due to the enzyme reaction at each of the wavelength. From

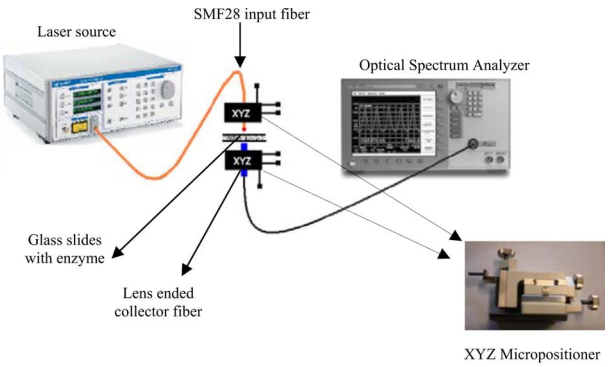

(a)

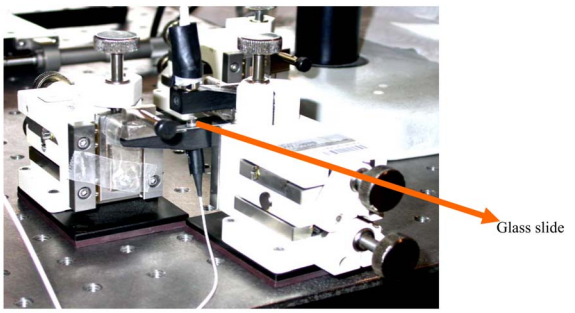

(b)

Fig. 6 (a) Schematic of the experimental setup for absorption measurement at 1550 nm and (b) experimental setup.

the maximum optical loss measured in decibels, the absorption coefficient was calculated as follows.

The expression for absorbance loss is given as

Table 1 Absorption coefficients for the HRP-H_2O_2 reaction at different wavelengths of light.

Wavelength of Light (nm)	Maximum Absorbance for HRP-H_2O_2 (1:1) Reaction	Loss (dB)	Absorption Coefficient (cm^{-1})
470	0.06	0.6	138.155
635	0.09	0.9	207.37
1550	0.3	3	690.77

$$\ln(P_{\text{output}}/P_{\text{input}}) = -\alpha_{\text{ab}} L_{\text{ab}}, \tag{3}$$

where α_{ab} is the absorbance coefficient, and L_{ab} is the absorbance length, which is the gap between the glass slides with the enzyme-antibody, measured to be $\sim 10\ \mu$m. The ratio $P_{\text{output}}/P_{\text{input}}$ is calculated from the loss in decibels, β_{ab}, obtained from the experimental results by the expression given as

$$\beta_{\text{ab}} = -10 \log(P_{\text{output}}/P_{\text{input}}). \tag{4}$$

Therefore, the expression relating the absorption coefficient and the propagation loss is given as

$$\beta_{\text{ab}} = (-10)(\alpha_{\text{ab}} l_{\text{ab}})[\log(e)]. \tag{5}$$

From the absorption experiments for different wavelengths of light, the absorption coefficient was computed for the maximum optical loss. The values are tabulated in Table 1. The results obtained from the absorbance measurements obtained from the experiments were compared with the previously published results.[28,30] In the published results, the concentration

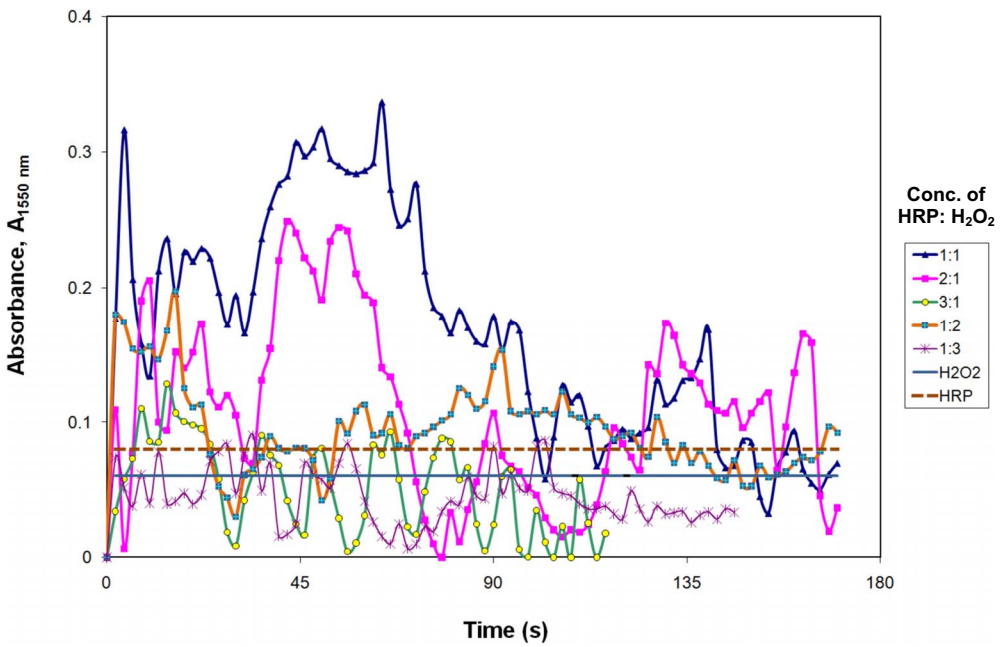

Fig. 7 Optical propagation loss with time at 1550 nm for different volumetric ratios of enzyme HRP and antibody H_2O_2.

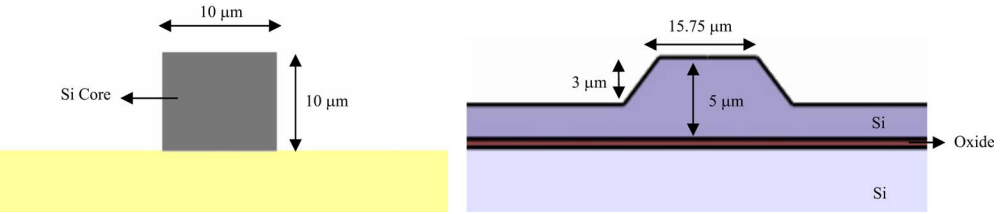

Fig. 8 Geometry of the square and the trapezoidal waveguides used for evanescence testing.

of the enzyme-antibody was not the same as the ones used in the present experiments. For example, Baek and Van Wart[28] used 1 μM HRP with 1 mM H_2O_2 in 50% methanol and obtained an absorbance value of ~0.03, which is close to the value of 0.035 obtained for absorbance measurements with H_2O_2 alone, as seen from Fig. 3. Similarly, the absorbance value of ~0.02, as reported by Akita et al.,[30] is the nearly the same value obtained when absorbance measurement experiments were carried out for H_2O_2 taken independently at a 635-nm wavelength. Therefore, it is evident that absorbance is maximum when specimens are taken in 1:1 volumetric ratio for the given molar concentrations of the specimen.

The preceding optical absorption experiments were useful in characterizing the activity of the biomolecules at different wavelengths and predicting the time taken for the reaction to be complete. As the molecular chains form during the reaction, the absorbance of light in the sample of enzyme-antibody increases. The absorbance reaches a certain peak after ~100 s when the reaction tends toward completion. After ~150 s, the ensuing absorption is due to the remnants of the samples. When the experiment is continued for a longer time, it can be observed that the absorption slowly starts decreasing. This phenomenon is due to the evaporation of the specimen. The results obtained with the optical absorption measurements at all wavelengths are consistent with the values predicted for the reaction time between HRP and H_2O_2.

It is also evident from the experiments that the biological pair exhibit maximum optical activity at a 1550-nm IR wavelength. The high sensitivity of the biomolecules to the IR wavelength provides confidence to employ the biological specimen for further examination using the IR light.

3 Evanescence Testing with SOI Waveguides

Two types of SOI waveguides were fabricated, namely, square waveguides and anisotropic trapezoidal waveguides. The rib SOI waveguides fabricated with the MicraGEM process technology[31] and the anisotropic waveguides were micromachined on SOI wafers with tetra methyl ammonium hydroxide (TMAH) using standard lithography. The main idea of fabricating two different types of waveguides was to study the feasibility of evanescence; while the inclined sidewalls of the waveguides offer more surface area for the immobilization on biomolecules, and hence greater possibility of evanescence, the square rib waveguides would exhibit evanescence only from the top surface of the waveguide. Thus, one could control the amount of evanescence by controlling the sidewall angle of the waveguide. The cross-sectional geometry of the square waveguide and the anisotropic waveguides is as shown in Fig. 8. The evanescence also depends on waveguide geometry and field distribution.

Figure 9 shows the biophotonic testing setup for evanescence measurement. The input light at 1550 nm was guided through a fiber from a laser source (Photonetics, Tunics BT). A tapered lens ended fiber (OZ optics, Ontario, Canada), which gives a spot size of 5 μm at a distance of 26 μm, was used as the input fiber. One end of the fiber was a fixed connection patch cord (FC-PC) connector and the other end was

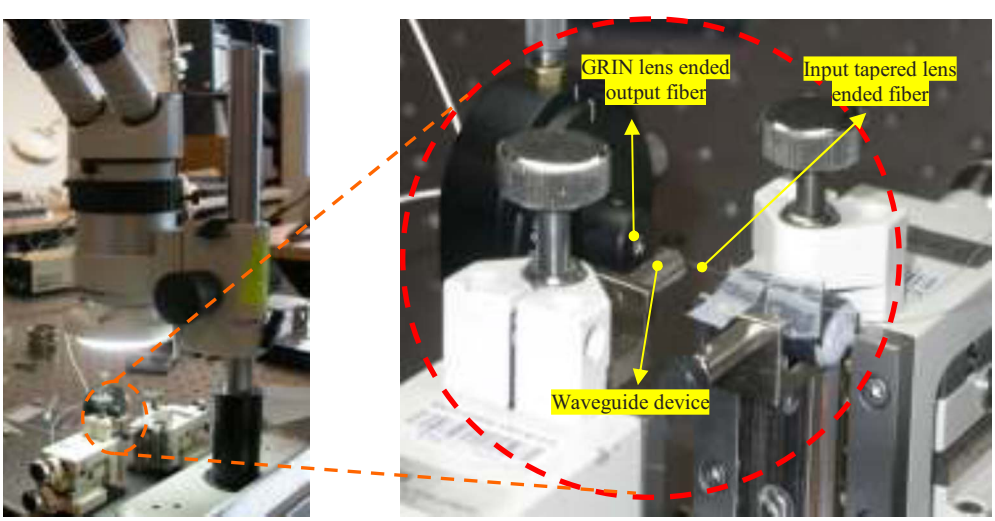

Fig. 9 Biophotonic testing setup developed at the Optical-Bio Microsystems laboratory.

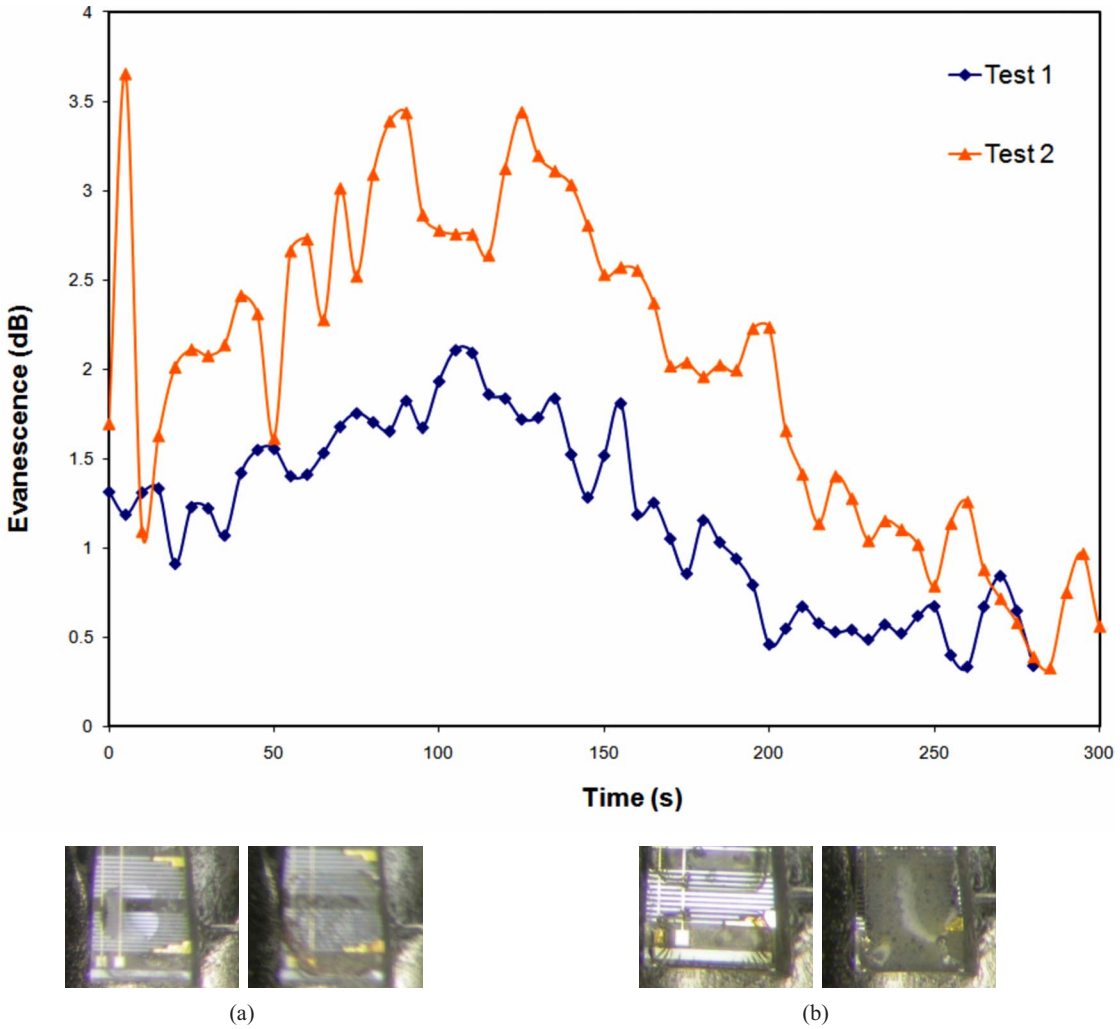

Fig. 10 Plot of the evanescence loss with time for HRP-H_2O_2 and the enzyme reaction on the waveguide as seen under the microscope for different trials of evanescence study: (a) test 1 and (b) test 2.

the tapered lens through which light is emitted into the waveguide. Both the tapered lens fiber and the waveguide device were mounted on individual *xyz* micropositioners so as to enable separate alignment of each module. The light coming out of the waveguide was collected using the GRIN lens mounted on an adjustable positioner. The GRIN-lens-ended fiber was connected to the OSA for the quantification of the power output. The alignment of the waveguide with respect to the fiber was carried out by observation under the microscope.

Initially, the position of the input fiber with respect to the GRIN lens was adjusted and the power output from the OSA was measured. Since a series of waveguides were fabricated on the single chip, when the position of the chip was altered laterally, it was easier to detect whether the light was being guided through the waveguide or being dispersed in free space, i.e., in the gap between the adjacent waveguides. Once the lateral alignment was perfectly carried out, the the vertical alignment was carried out.

The biomolecules were added using a precision volume pipette (Gilson). After testing, the waveguide was cleaned using isopropyl alcohol (IPA). The surface was again cleaned with deionized (DI) water and introduced in a flux of pure nitrogen gas to dry out the water and prepare the waveguide surface for evanescence testing again.

3.1 *Results*

The experiments were repeated for a sufficient number of times without the effect of absorbance, and the results showed the optical loss purely due to evanescence. On SOI rectangular rib waveguides, two successful experiments were conducted isolating the effect of complete absorption of the light by the enzymes, for the rectangular waveguides. The results of optical evanescence are plotted in Fig. 10 along with the corresponding images of the reaction. H_2O_2 was passively immobilized on the surface of the waveguide and HRP was subsequently added to start the instantaneous reaction.

The trend for evanescence is similar for tests 1 and 2. However, the evanescent field length is different for both these cases, as seen from the images taken during the reaction, which is believed to have caused the difference in evanescence loss measured. In case of test 1, H_2O_2 was added initially and then HRP was added to the antibody. However, in test 2, H_2O_2 was added subsequently after HRP was added

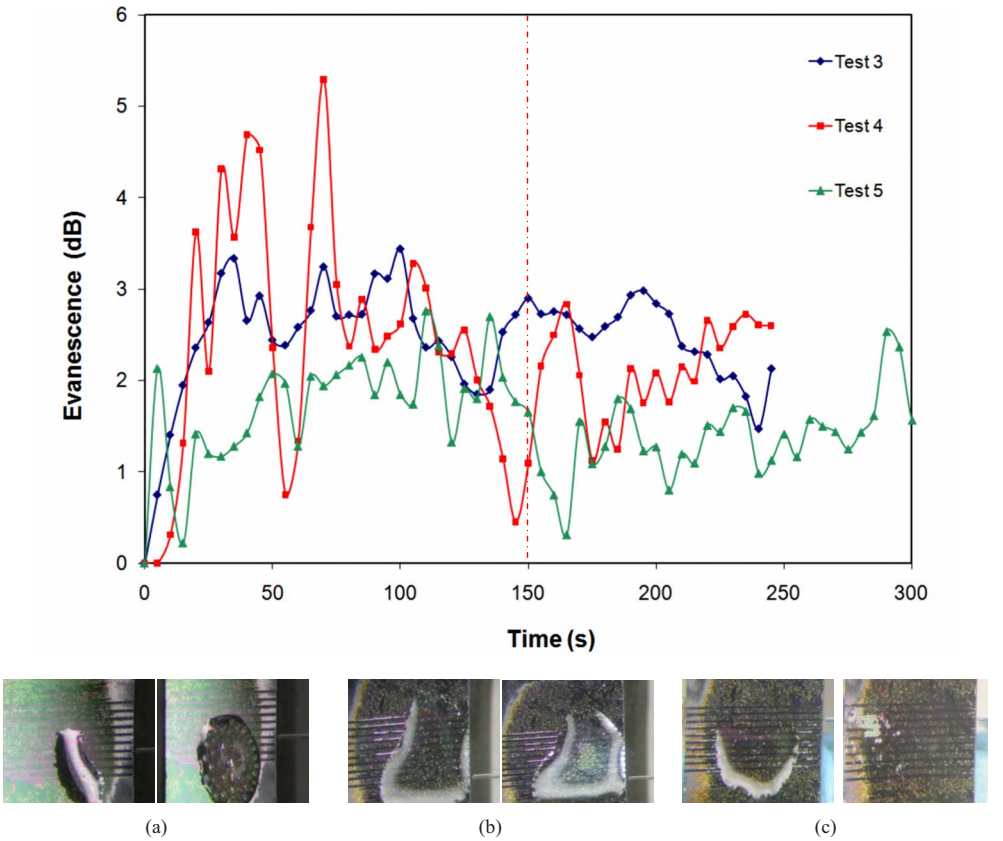

Fig. 11 Plot of evanescence loss with time for the reaction between HRP and H_2O_2 on anisotropic silicon waveguide with taper angle 35.26 deg in (a) test 3, (b) test 4, and (c) test 5.

initially, to check the evanescence due to HRP alone initially and then due to the reaction.

In the next series of experiments, anisotropic trapezoidal waveguides were used to demonstrate the evanescence. Waveguides with sidewalls inclined at 35.26 deg were used for the experiments. The testing setup was the same one as used with the rectangular waveguide devices. The antibody was immobilized on to the surface of the waveguide and HRP was added subsequently. The results of the evanescence study are plotted in Fig. 11 along with the respective photographs of the device during testing.

Given the irregularities in the microfabrication along with the multimode nature of the waveguide, the loss of light propagating through the waveguide was considerable. However, the evanescence trend for the enzyme reaction is seen in all the tests and the variation in evanescent loss is mainly due to the roughness scattering. The time taken for the reaction, ~150 s, as observed from the evanescence measurements corroborates well with the reaction time predicted by the optical absorption measurements reported in Sec. 2.4.

3.2 *Calculation of Evanescence Coefficient*

From the loss observed in the waveguides due to the enzyme reaction, the evanescence coefficient of the HRP-H_2O_2 reaction was calculated to standardize the evanescence measured by the rectangular and the anisotropic SOI waveguides. The following procedure was adopted in calculating the evanescence loss for the calculation of evanescence coefficient.

From the results of the experiments that were carried out by adding HRP and H_2O_2 individually and measuring the power loss, the evanescent loss coefficient was computed for

Table 2 Evanescent coefficient for the different tests carried out on the rectangular rib waveguides for the HRP-H_2O_2 reaction.

Experiment with Rectangular Waveguides	Maximum Evanescent Loss (dB)	Average Evanescent Loss (dB)	Length of the Waveguide Evanescent Field (μm)	Evanescent Loss (dB/cm)	Evanescent Coefficient for the Enzyme Reaction (cm^{-1})
Test 1	2.108	1.519	720	12.655	2.91
Test 2	3.656	2.75	1200	22.01	5.067

Table 3 Evanescent coefficient for the different tests carried out on the anisotropic SOI waveguides for the HRP-H_2O_2 reaction.

Experiment with Anisotropic Waveguide	Maximum Evanescent Loss (dB)	Average Evanescent Loss (dB)	Evanescent Field Length (μm)	Evanescent Loss (dB/cm)	Evanescent Coefficient of the Enzyme Reaction (cm^{-1})
Test 3	3.43	2.89	988	8.79	2.02
Test 4	5.289	2.48	3300	7.515	1.73
Test 5	2.65	1.65	2541	6.493	1.49

each of the specimen. The length of the waveguide was measured to be 1320 μm. The individual evanescent field lengths of the enzymes were measured from the corresponding images taken under the microscope. If the evanescent length of the waveguide covered by the specimen, in micrometers, be denoted by L_{ev}, and the optical power loss in decibels measured after the addition of the specimen due to evanescence be ΔP_{ev}, the evanescence loss in decibels per centimeter is given by the relation

$$\beta_{ev}(\text{dB/cm}) = (\Delta P_{ev}/L_{ev}) \times 10^4. \quad (6)$$

For the computation of the evanescence coefficient, it is assumed that evanescent field length over which the reaction occurs is the length of the waveguide over which the antibody was immobilized initially. Accordingly, the total loss due to evanescence was computed by the following relations.

$$\text{Total evanescent loss } \beta_{ev}(\text{dB/cm}) = \beta_{rn} L_{rn}. \quad (7)$$

Here β_{rn} is taken as the evanescence due to enzyme reaction. The length covered by the reacting enzymes, L_{rn}, is assumed to be the same length of the waveguide covered by the antibody added initially. From Eqs. (6) and (7), the evanescent coefficient was calculated as

$$\beta_{ev} = (10)(\alpha_{ev})[\log_{10}(e)], \quad \therefore \ \alpha_{ev} = \beta_{ev}/\{(10)[\log_{10}(e)]\}. \quad (8)$$

Here the evanescent loss is taken as the maximum power loss observed during the reaction. The values of the evanescence coefficient obtained from the different experiments are tabulated in Table 2.

For the anisotropic waveguides, a similar calculation was carried out and the evanescence coefficient was calculated as given in Table 3. A second degree polynomial trend line was added through the data points obtained and the peak of the trend line is taken as the average evanescence value.

Figure 12 shows the scanning electron microscopy (SEM) images of the waveguide surface with the different specimen. It is assumed that when hydrogen peroxide is passively immobilized on the surface of the waveguides, an active biological layer is formed on the surface. Subsequently, on the addition of the HRP, the active molecules react with the immobilized hydrogen peroxide molecule present on the surface of the waveguide and the redox reaction would result in the formation of the compound as seen in Fig. 12(c). When the light is guided through the waveguide, the bio-optical interaction of the evanescent tail of light and the biological reactions which take place at the surface of the waveguide causes evanescence loss, which gives the characteristics of the reaction.

Thus, the biodetection has been demonstrated through the method of evanescence on an SOI platform. Even though the results do not predict the evanescence coefficients of the biomolecules to pinpoint accuracy, the feasibility of biodetection using evanescence principle in infrared wavelength has been well established. The bio-optical interaction can be precisely controlled and the waveguide geometry can now be tuned to achieve more accurate evanescence coefficients for specific biological specimen, depending on their optical activity. This technique can now be further extended to identify other biological specimen and the evanescent wave optical detection system can be suitably integrated with other modules for the fabrication of a fully integrated μTAS, which would be useful in several medical applications.

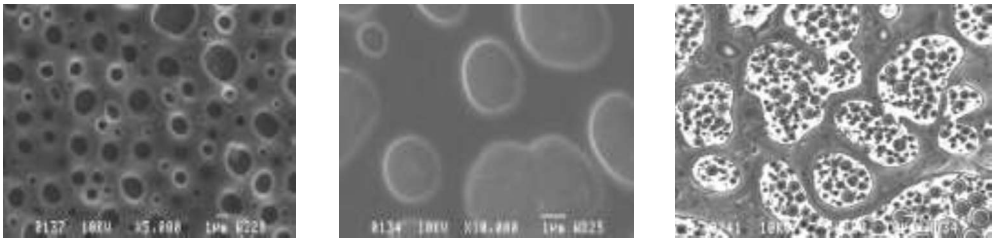

(a) (b) (c)

Fig. 12 SEM images of the waveguide surface with (a) H_2O_2, (b) HRP, and (c) HRP-H_2O_2.

4 Conclusion

A label-free biophotonic detection method using the principle of evanescence on waveguides was proposed for the detection of active chemical and biological species. Optical activity of the biomolecules in different wavelength ranges was characterized by absorption measurements. Experiments were then carried out on the rectangular rib waveguides and the anisotropically etched SOI waveguides for biosensing through the bio-optical interaction caused due to the evanescent waves. The main novelties of this work are the development of platform for biosensing in the near-IR wavelength using silicon, the capability of carrying out controlled chemical and biological sensing with the proposed system depending on the bio-optical interaction brought about due to the activity of the target specimen, and the feasibility of integrating these miniaturized waveguide-based devices onto a μTAS. Silicon carries with itself certain distinct advantages and is turning out to be a useful and cost-effective material for bulk fabrication of an effective biosensor. Silicon waveguides can be miniaturized from the order of nanometers to a few micrometers to achieve a single-mode condition for the wave propagation. The commercially viable advantages of using a silicon platform are cost effectiveness and ease of microfabrication through different fabrication techniques such as bulk micromachining, surface micromachining, and deep reactive ion etching (DRIE). Another advantage of using the IR light is that the wavelength is compatible with silicon, and this opens up the feasibility of integrating the biosystem with the telecommunication technology for several applications. Thus, the proposed evanescence-based biodetection technique on a silicon platform is very useful for the fabrication of fully integrated μTHS, which can be used for several point-of-care testing applications and *in situ* biomedical diagnoses.

References

1. S. C. Jakeway, A. J. de Mello, and E. L. Russell, "Miniaturized total analysis systems for biological analysis," *Fresenius' J. Anal. Chem.* **366**, 525–539 (Mar–Apr. 2000).
2. D. R. Reyes, D. Iossifidis, P. A. Auroux, and A. Manz, "Micro total analysis systems. 1. Introduction, theory, and technology," *Anal. Chem.* **74**, 2623–2636 (June 15, 2002).
3. P. A. Auroux, D. Iossifidis, D. R. Reyes, and A. Manz, "Micro total analysis systems. 2. Analytical standard operations and applications," *Anal. Chem.* **74**, 2637–2652 (June 15, 2002).
4. T. Vilkner, D. Janasek, and A. Manz, "Micro total analysis systems. Recent developments," *Anal. Chem.* **76**, 3373–3385 (June 15, 2004).
5. P. S. Dittrich, K. Tachikawa, and A. Manz, "Micro total analysis systems. Latest advancements and trends," *Anal. Chem.* **78**, 3887–3908 (June 15, 2006).
6. M. Zourob, S. Mohr, P. Fielden, and N. Goddard, "Small-volume refractive index and fluorescence sensor for micro total analytical system (mu-TAS) applications," *Sens. Actuators B* **94**, 304–312 (2003).
7. M. A. Schwarz and P. C. Hauser, "Recent developments in detection methods for microfabricated analytical devices," *Lab Chip* **1**, 1–6 (Sep. 2001).
8. M. Yuqing, G. Jianguo, and C. Jianrong, "Ion sensitive field effect transducer-based biosensors," *Biotechnol. Adv.* **21**, 527–534 (2003).
9. H. Ayliffe, A. Frazier, and R. Rabbitt, "Electric impedance spectroscopy using microchannels with integratedmetal electrodes," *J. Microelectromech. Syst.* **8**, 50–57 (1999).
10. O. Leistiko and P. F. Jensen, "Integrated bio/chemical microsystems employing optical detection: the clip-on," *J. Micromech. Microeng.* **8**, 148–150 (1998).
11. J. Amritsar, I. G. Stiharu, M. Packirisamy, G. Balagopal, and X. Li, "MOEMS-based cardiac enzymes detector for acute myocardial infarction," *Proc. SPIE* **5578**, 91–98 (2004).
12. A. Jeetender, I. Stiharu, and M. Packirisamy, "MOEMS for bioenzymatic detection," *Photon. Tech. Rev. CIPI* **3**(1), 25–27 (2005).
13. J. Amritsar, I. Stiharu, and M. Packirisamy, "Bioenzymatic detection of troponin C using micro-opto-electro-mechanical systems," *J. Biomed. Opt.* **11**, 021010 (Mar.–Apr. 2006).
14. N. Menon, L. ChromoLogic, and N. Corning, "Optical biosensors: applying photonics products to biomedical diagnostics market," in *Proc. Optical Fiber Communication Conf.*, Vol. **2** (2004).
15. K. B. Mogensen, J. El-Ali, A. Wolff, and J. P. Kutter, "Integration of polymer waveguides for optical detection in microfabricated chemical analysis systems," *Appl. Opt.* **42**, 4072–4079 (July 1, 2003).
16. S. Balslev, A. M. Jørgensen, B. B. Olsen, K. B. Mogensen, K. B. Mogensen, D. Snakenborg, O. Geschke, J. P. Kutter, and A. Kristensen, "Lab-on-a-chip with integrated optical transducers," *Lab Chip* **6**, 213–217 (2006).
17. S. Balslev, B. Bilenberg, O. Geschke, A. Jorgensen, A. Kristensen, J. Kutter, K. Mogensen, and D. Snakenborg, "Fully integrated optical system for lab-on-a-chip applications," in *Proc. 17th IEEE Int. Conf. on Micro Electro Mechanical Systems, 2004*, pp. 89–92 (2004).
18. G. Minas, R. F. Wolffenbuttel, and J. H. Correia, "A lab-on-a-chip for spectrophotometric analysis of biological fluids," *Lab Chip* **5**, 1303–1309 (Nov. 2005).
19. J. R. Webster, M. A. Burns, D. T. Burke, and C. H. Mastrangelo, "Monolithic capillary electrophoresis device with integrated fluorescence detector," *Anal. Chem.* **73**, 1622–1626 (Apr. 1, 2001).
20. L. Cui, T. Zhang, and H. Morgan, "Optical particle detection integrated in a dielectrophoretic lab-on-a-chip," *J. Micromech. Microeng.* **12**, 7–12 (2002).
21. J. M. Ruano, A. Glidle, A. Cleary, A. Walmsley, J. S. Aitchison, and J. M. Cooper, "Design and fabrication of a silica on silicon integrated optical biochip as a fluorescence microarray platform," *Biosens. Bioelectron.* **18**, 175–184 (2003).
22. R. Mazurczyk, J. Vieillard, A. Bouchard, B. Hannes, and S. Krawczyk, "A novel concept of the integrated fluorescence detection system and its application in a lab-on-a-chip microdevice," *Sens. Actuators B* **118**, 11–19 (2006).
23. A. Densmore, D. X. Xu, P. Waldron, S. Janz, P. Cheben, J. Lapointe, A. Delge, B. Lamontagne, J. Schmid, and E. Post, "A silicon-on-insulator photonic wire based evanescent field sensor," *IEEE Photon. Technol. Lett.* **18**, 2520–2522 (2006).
24. A. Jeetender, I. Stiharu, and M. Packirisamy, "Micro-opto mechanical biosensors for enzymatic detection," *Proc. SPIE* **5969**, 59690V (2005).
25. M. Tanaka, K. Matsuura, S. Yoshioka, S. Takahashi, K. Ishimori, H. Hori, and I. Morishima, "Activation of hydrogen peroxide in horseradish peroxidase occurs within approximately 200 micro s observed by a new freeze-quench device," *Biophys. J.* **84**, 1998–2004 (Mar. 2003).
26. R. K. DiNello and D. H. Dolphin, "Substituted hemins as probes for structure-function relationships in horseradish peroxidase," *J. Biol. Chem.* **256**, 6903–6912 (July 10, 1981).
27. B. Lu, E. I. Iwuoha, M. R. Smyth, and R. O'Kennedy, "Effects of acetonitrile on horseradish peroxidase (HRP)-anti HRP antibody interaction," *Biosens. Bioelectron.* **12**, 619–625 (1997).
28. H. K. Baek and H. E. Van Wart, "Elementary steps in the formation of horseradish peroxidase compound I: direct observation of compound 0, a new intermediate with a hyperporphyrin spectrum," *Biochemistry* **28**, 5714–5719 (July 11, 1989).
29. A. Chandrasekaran and M. Packirisamy, "Absorption detection of enzymatic reaction using optical microfluidics based intermittent flow microreactor system," *IEE Proc.: Nanobiotechnol.* **153**, 137–143 (Dec. 2006).
30. M. Akita, D. Tsutsumi, M. Kobayashi, and H. Kise, "Structural change and catalytic activity of horseradish peroxidase in oxidative polymerization of phenol," *Biosci., Biotechnol., Biochem.* **65**, 1581–1588 (2001).
31. A. Chandrasekaran and M. Packirisamy, "Wafer dicing strategic planning technique for clustered BioMEMS devices," *Int. J. Prod. Develop.* **4**, 296–309 (2007).